
FOCUS: First Order Concentrated Updating Scheme

Yizhou Liu¹ Ziming Liu¹ Jeff Gore¹

Abstract

Large language models (LLMs) demonstrate remarkable performance, and improving their pre-training process appears to be key to enhancing their capabilities further. Based on the documented success of Adam, learning rate decay, and weight decay, we hypothesize that the pre-training loss landscape features a narrowing valley structure. Through experiments with synthetic loss functions, we discover that when gradient query noise is high relative to the valley’s sharpness, Adam’s performance falls behind that of Signum because Adam reduces the effective step size too drastically. This observation led us to develop FOCUS, an optimizer that enhances Signum by incorporating attraction toward moving averaged parameters, allowing it to handle noise better while maintaining larger step sizes. In training GPT-2, FOCUS proves to be more stable than Signum and faster than Adam. These results suggest that gradient noise may be an underappreciated limiting factor in LLM training, and FOCUS offers promising solutions.

1. Introduction

The emergence of large language models (LLMs) represents a transformative advancement in artificial intelligence. These systems have demonstrated remarkable capabilities that extend far beyond their initial purpose of processing and generating human language. From engaging in nuanced conversations and crafting creative content (Brown et al., 2020; OpenAI, 2023; Qin et al., 2023) to solving complex mathematical problems (Lewkowycz et al., 2022; Taylor et al., 2022; Wolfram, 2023; Trinh et al., 2024) and assisting with software development (Chen et al., 2021; GitHub, 2022), LLMs continue to expand the boundaries of what artificial intelligence can achieve.

To further advance the capabilities of LLMs, improving the pre-training is a critical research direction (Kaplan et al.,

2020; Hoffmann et al., 2022; Liu et al., 2023a). Better optimizers are desired to reduce time, cost, model size, etc. for reaching the same loss or to achieve lower losses given similar budgets. To this end, it is essential to understand the loss landscapes in LLM pre-training and design optimizers accordingly.

To gain insights into the training dynamics, we take the physicists’ approach of simplifying the real world into a picture and a toy model (Figure 1a). A picture describes only the important features and ignores all other details. A toy model then specifies the picture with quantification. We can gain insights and generate testable hypotheses through a systematic study of the toy model. Then, we can apply our insights to engineer the real systems or we may fail and update our picture.

In this paper, we start in Section 2.1 to build a picture for pre-training landscapes, i.e., a narrowing valley (Figure 1b), based on previous results (Wei & Schwab, 2019; Liu et al., 2023a; Wen et al., 2024). Depending upon the topology of the loss landscape, different optimizers may respond differently. We next construct loss landscapes and study the behaviors of different optimizers in Section 2.2. We find when the noise in gradient is too large (see an example in Figure 1c), Adam (Kingma & Ba, 2014; Loshchilov & Hutter, 2019) performs worse than Signum (Bernstein et al., 2018) which takes constant size steps based on the sign of the momentum (smoothed gradient). Adam decreases its effective step size too much when the gradient is too noisy while Signum fixes the step size. Inspired by this observation, we designed the FOCUS optimizer by adding an attraction force towards the moving averaged parameters to Signum, so that FOCUS can squeeze into valleys with fixed step sizes (see Section 2.3). In GPT-2 (small) pre-training, FOCUS is more stable than Signum and Adam with similar learning rates. FOCUS is favored compared to Adam (Figure 1d), achieving a twice speedup compared to Adam from the literature in terms of training time (see details in Section 3). We provide a convergence analysis of FOCUS in Section 4, discuss related works in Section 5, and conclude with physics intuitions in Section 6.

Our results contribute to both **scientific understanding** of training dynamics and **practical speedup** in LLM pre-training. We propose a minimal model with sharp valley

¹Massachusetts Institute of Technology, Cambridge, MA 02139, USA. Correspondence to: Yizhou Liu <liuzy@mit.edu>.

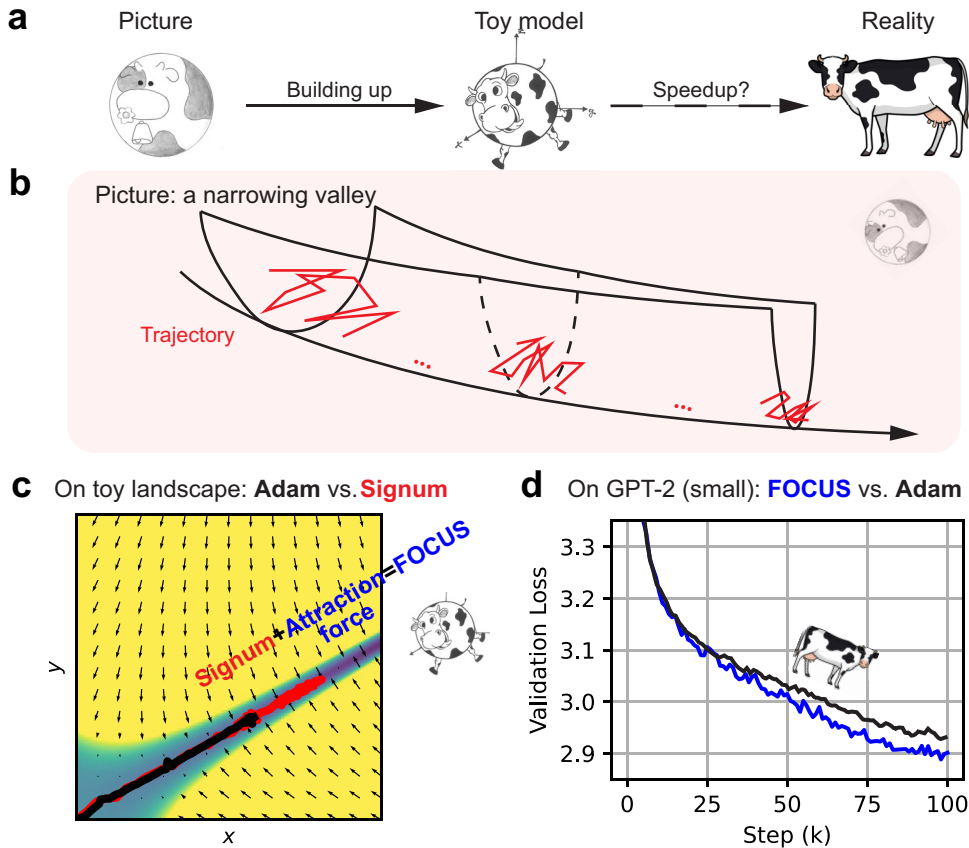


Figure 1. Insights from toy models lead to practical speedup in LLM pre-training. (a) Our philosophy that a simple and self-consistent picture provides a basis of thinking and testable hypotheses is not necessarily correct. Interactions between testing the real world and updating our picture keep us moving forward. (b) Narrowing valleys are assumed to be a key structure in LLM training loss. (c) The toy model explains that Adam can be slow with a large gradient noise (Section 2). (d) By adding self-attraction to Signum, FOCUS is proposed to handle sharp landscapes with large gradient stochasticity and achieve practical speedups (Section 3).

and gradient noise to study training dynamics. We obtain a better understanding of Adam’s advantage in handling the sharpness and its limitation when gradient noise is large. Finally, we propose FOCUS using attraction force to squeeze into valleys without decreasing effective step size much, which gains actual speedup in training GPT-2 (small). We anticipate that FOCUS will provide new insights and directions for designing optimizers that will inspire a variety of new optimizers.

2. Methods

2.1. Picture of loss landscapes

In this part, we first describe the narrowing valley picture depicted in Figure 1b and then explain why this picture is relevant to the actual pre-training losses of LLMs.

A valley structure means heterogeneous curvatures across

parameter dimensions. There are many sharp and flat dimensions, where the sharp ones form the walls of the valley and the valley extends along the flat ones (Figure 1b). Going down along the valley, one obtains lower loss. However, the sharp directions may be sharper or more. For an optimizer, it is easy to find the bottom of one valley along the sharp directions, but it may be challenging to stay at the bottom and follow the flat directions to move forward. We summarize the picture of the loss landscape as a “narrowing valley”.

The evidence for heterogeneous curvatures is explained as follows. A direct study of Hessian of GPT-2 supports our picture (Liu et al., 2023a). Theory suggests that large uncertainty variation in data distribution can lead to heterogeneous curvatures (Wen et al., 2024), which is likely to be true in language as the same phrase can naturally have many different continuations. A piece of side evidence is that Adam and its variants were shown to outperform stochastic gradient descent (SGD) in LLM training (Zhao et al., 2024).

Adam is better at dealing with heterogeneous directions since it normalizes the updates in different parameter directions to be of the same order of magnitude. However, SGD can be extremely slow along the flat directions if it wants convergence along the sharp directions (Liu et al., 2023a).

Another important feature is that the valley is getting narrower and narrower. We conjecture this property due to the success of some learning rate schedulers (Loshchilov & Hutter, 2017; Jin et al., 2023; Subramanian et al., 2024): decreasing learning rate at the late stage of training can help to reach a lower loss. Due to the discretized nature of optimizers, a smaller learning rate is needed for convergence given larger curvature (Liu et al., 2023a). For optimizers like Adam, a smaller learning rate helps to be close to the bottom, especially at places with large curvatures. In the continuous limit, learning rates also play the role of temperature (Shi et al., 2020; Liu et al., 2023b) and decreasing temperature makes “bouncing particles” easier to squeeze into sharper valleys. According to different heuristics and theories, the fact that lowering learning rates works supports the narrowing valley picture.

Compared to the conventional picture of the loss landscapes, one important difference is that we do not draw the minimum (Figure 1b). We are assuming that the true minimum is far from being reached. This is inspired by the fact that lowering weight decay can still result in larger parameter norms in current LLM pre-training (Andriushchenko et al., 2024; Wang & Aitchison, 2024). This feature also indicates that the valley should be narrower when moving forward. Otherwise, the optimizer should reach the minimum easily even when far away.

Besides the key ingredients introduced, there are several factors worth mentioning. First, the loss function is defined by the distribution of data. Due to the finite batch size, the gradient obtained can be thought of as the gradient of the landscape with some noise. Second, the valley structure is one elementary ingredient. The landscape can be highly non-convex by having many valleys. As explained in Introduction (Section 1), our picture keeps the simplified fundamental structure and updates details when the original one does not suffice. Finally, the picture merits study in its own right, independent of its applications to optimization. The picture offers a base of thinking and can help to generate all kinds of techniques and testable hypotheses. The picture is also open to modifications based on feedback from experiments on real systems.

2.2. Toy model

In this section, we present our toy landscapes in the spirit of “narrowing valleys” and then our insights gained from the experiments.

Our toy loss function defined on x and y (can be thought of as model parameters) is given by

$$L(x, y) = \frac{a}{2}u^2v^2 - cu, \quad (1)$$

where u and v depends on x and y via a rotation, a and c are two hyperparameters controlling the loss. The valley direction is in general not aligned with the model parameters. Figure 1c depicts an example of the loss where u is rotated counter-clockwise from x by $\pi/6$. The term $-cu$ ($c > 0$) ensures that $+u$ is the direction along the valley to lower loss values. The curvature of the orthogonal direction v is given by au^2 which is getting larger when moving along the valley (going to greater u).

Upon building the landscape, we start our exploration with the small motivating question—why can Signum be comparable to Adam in LLM pre-training (Zhao et al., 2024)? Adam updates its parameters by $-\eta\hat{m}_t/\sqrt{\hat{v}_t}$ at step t (Kingma & Ba, 2014), where η is the learning rate, \hat{m}_t is the centered exponential moving average (EMA) of gradient, and \hat{v}_t is the centered EMA of the squared gradient. Specifically, we have

$$m_t = m_{t-1}\beta_1 + (1 - \beta_1)g_t, \quad (2)$$

where g_t (a vector) is the gradient queried at step t and $0 < \beta_1 < 1$ is a hyperparameter controlling how fast old gradients are forgotten. Similarly, we have

$$v_t = v_{t-1}\beta_2 + (1 - \beta_2)g_t^2. \quad (3)$$

All operations on vectors are element-wise. The centered averages \hat{m}_t and \hat{v}_t are normalized from m_t and v_t , respectively, since the initialization $m_0 = v_0 = 0$ introduces bias towards 0 (Kingma & Ba, 2014). The idea is that along sharp directions, corresponding elements in g_t may bounce around 0 such that $\hat{m}_t/\sqrt{\hat{v}_t}$ is small and the effective step size is small along those directions. While for flat directions, corresponding elements in g_t are consistent across different t , then $\hat{m}_t/\sqrt{\hat{v}_t}$ can be large or even close to 1. By construction, Adam is good at squeezing into narrowing valleys. Throughout the paper, when we need to add weight decay, we follow the method in AdamW (Loshchilov & Hutter, 2019).

Signum can be considered a simplified version of Adam that only uses momentum. Signum updates the parameters by $-\eta\text{sign}(\hat{m}_t)$ at step t . Signum uses fixed step size, losing the ability to adjust step size based on sharpness or the degree of query noise. Consequently, we would expect Signum to oscillate more violently and perform much worse than Adam in sharp valleys.

However, this expectation is not always true (Zhao et al., 2024). We compare Signum and Adam on our toy landscape to get possible explanations for the phenomenon. First of

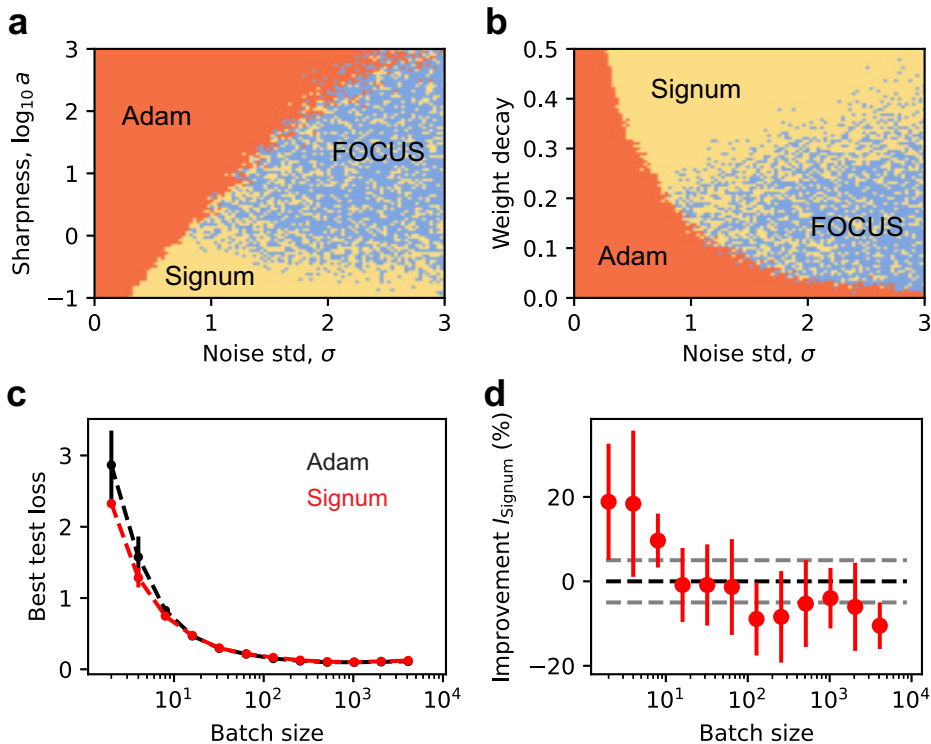


Figure 2. Signum outperforms Adam when gradient stochasticity is relatively large, and FOCUS further improves Signum when the valley-like landscape is sharp. (a) Signum outperforms Adam when gradient noise is large compared to sharpness. Orange pixels refer to conditions Adam is better and yellow parts mean Signum is better. FOCUS is even better than Signum after increasing sharpness. Blue pixels refer to conditions FOCUS is the best. (b) Increasing weight decay helps Signum and FOCUS against Adam. Yet the advantage of self-attraction is lost when weight decay is too large. (c and d) Gradient noise is large when batch size is small in practice. For MNIST classification, We find that increasing batch size (decreasing noise) can lead to a transition of the optimal optimizer from Signum to Adam, showing the insights from toy models are relevant to reality. Grey dashed lines in (d) highlight $\pm 5\%$. The error bars represent standard deviations. Experiment details are in Appendix A.

all, we indeed find that Signum can be faster than Adam and can squeeze into deeper places along the valley under the same hyperparameter settings (Figure 1c). We discovered this case when examining the effect of noise in gradient estimation, e.g., due to finite batch sizes. We model this stochasticity by multiplying the true gradient of the loss Equation (1) by a random variable with mean 1 and standard deviation σ when the gradient is queried. We obtain a hypothesis that large noise may change the competition between Adam and Signum.

Next, we compare Adam and Signum more systematically and fairly. As explained in Zhao et al. (2024), different optimizers can have different optimal learning rates and we need to compare their best performances with their own best hyperparameters. Given a loss function, we scan 20 learning rates between 10^{-3} and 1.0 (uniform in log scale) for each optimizer. We run 50 optimization tests for each learning rate where each test starts near the origin and runs for 10^3 steps. The optimal learning rate is selected via the mean of

final losses, typically around 10^{-2} .

In Figure 2a, we examine the best performance of different optimizers at different valley sharpness, a , and noise standard deviation, σ ($c = 0.1$ is set to be constant). The orange region refers to the parameters where Adam is the best and the yellow region for those where Signum is the best. We find that given sharpness a there is a critical noise strength σ_c beyond which Signum will become better than Adam. Moreover, this critical noise strength σ_c increases when sharpness a increases. Intuitively, both large sharpness (violent oscillation) and large noise lead to a small signal-to-noise ratio $\hat{m}_t/\sqrt{\hat{v}_t}$. When a small signal-to-noise ratio is mainly due to sharpness, the small effective step size helps to get into the valley, and Adam is therefore faster. However, when a small signal-to-noise ratio is mainly due to noise, Adam decreases the effective step size too much and becomes slower. A small step size also makes Adam stop at a place closer to the origin given the same weight decay. We conclude that Signum outperforms Adam when

the gradient noise is large compared to the sharpness of the valley.

For completeness, we should also compare the performance of optimizers at their best weight decays (another hyperparameter they all have). On our toy landscape, the smaller the weight decay is, the better the performance will be, which is true for all optimizers tested. However, training LLM usually does not set zero weight decay for many reasons (Andriushchenko et al., 2024). Some non-zero small weight decay is needed for other aspects not described by our toy model. And the smallest possible weight decay will be the optimal one for all optimizers in terms of final loss. We then can choose that value for weight decay and compare different optimizers with their own best learning rates. Since the smallest possible weight decay is some unknown value, we test different weight decay values (Figure 2b). We find no matter which weight decay is used, small noise prefers Adam and large noise prefers Signum as before. And at the same degree of stochasticity, Signum is favored at larger weight decay. Large weight decay may help Signum to be stable and stay closely in the valley. We conclude from our toy model experiments that at various conditions, Signum outperforms Adam when the noise in gradients is relatively large.

Finally, we try to test our findings from the toy model on real optimization problems. In particular, the noise of gradient queries in the toy model is artificial yet is believed to be related to finite batch size in real problems. We then would like to check whether in reality there is a transition from Signum outperforming Adam to Adam outperforming Signum when increasing batch sizes (decreasing gradient stochasticity). We use a six-layer multilayer perceptron (see Appendix A.2 for details) to do MNIST classification (LeCun et al., 1998). Given the batch size, we find the optimal learning rate for each optimizer by scanning 20 learning rates from 10^{-4} to 1.0 uniformly in log scale. For each learning rate, we run three replicates and each run has 400 steps to ensure saturation. Each learning rate has a mean final loss over replicates and the best test loss is chosen from these mean final losses of different learning rates. The best test loss of Adam indeed is larger than that of Signum at small batch sizes but becomes smaller than that of Signum after the batch size gets large (Figure 2c). This trend agrees with our insights obtained from the toy model. We define the improvement of Signum as

$$I_{\text{Signum}} = \frac{L_{\text{Adam}} - L_{\text{Signum}}}{L_{\text{Adam}}}, \quad (4)$$

where L_{Adam} and L_{Signum} are best losses of Adam and Signum, respectively. The improvement I_{Signum} captures the transition from Signum being better to Adam being better when increasing batch sizes (Figure 2c). We conclude that our finding on toy landscapes about the competition

Algorithm 1 FOCUS (All operations on vectors are element-wise and β_2^t means β_2 to the power t)

Input: Initial parameter vector θ_1 , learning rate $\{\eta_t\}_{t=1}^T$, hyperparameters $\beta_1, \beta_2, \gamma, \omega$
Set $m_0 = 0, \bar{\theta}_0 = 0$
for $t = 1$ **to** T **do**
 Compute minibatch loss $L_t(\theta_t)$
 Obtain gradient $g_t = \nabla L_t(\theta_t)$
 $m_t = \beta_1 m_{t-1} + (1 - \beta_1)g_t$ (Update biased momentum)
 $\bar{\theta}_t = \beta_2 \bar{\theta}_{t-1} + (1 - \beta_2)\theta_t$ (Update biased average parameters)
 $\hat{\theta}_t = \bar{\theta}_t / (1 - \beta_2^t)$ (Compute bias-corrected average parameters)
 $\theta_t = \theta_t - \eta_t \omega \hat{\theta}_t$ (Apply weight decay)
 $\theta_{t+1} = \theta_t - \eta_t (\text{sign}(m_t) + \gamma \text{sign}(\theta_t - \hat{\theta}_t))$
end for

between Adam and Signum is relevant to realistic machine learning problems.

2.3. FOCUS optimizer

Good insights into the training dynamics should lead to practical speedup. To this end, we try to design new optimizers based on what we learned from the toy model experiments. On the one hand, we want the new optimizer not to decrease the effective step size like Adam such that it can work well when gradient noise is large. On the other hand, we want the optimizer to be able to squeeze into the sharp valley. We then try to add some new mechanisms to Signum for better dealing with sharpness. Imagining the picture Figure 1b, we want the trajectory to be more compact. One way to realize that is to add an attraction force between the ‘‘bouncing particles’’, i.e., parameter values at different time steps.

One realization of adding an attraction force term to Signum is our FOCUS (First Order Concentrated Updating Scheme) optimizer in Algorithm 1. The optimizer queries 0th and 1st order information. We use the word ‘‘concentrated’’ to highlight the attraction force term. Upon getting gradient g_t , FOCUS updates the EMA of gradient, m_t , which is called momentum, as well as the EMA of parameters, $\bar{\theta}_t$. The hyperparameters $\beta_1, \beta_2 \in [0, 1)$ are the decay rates of the EMAs of gradients and parameters, respectively. Since we initialize $\bar{\theta}_0 = 0$, we need normalization $\hat{\theta}_t = \bar{\theta}_t / (1 - \beta_2^t)$ to have an unbiased estimation of the moving average of parameters (Kingma & Ba, 2014). We do not compute bias-corrected momentum since we only need the sign later and normalization does not change the sign. We update the parameters by $-\eta_t \text{sign}(m_t)$ which follows Signum and by $-\eta_t \gamma \text{sign}(\theta_t - \hat{\theta}_t)$ which is the attraction force term. The hyperparameter $\gamma \in [0, 1)$ controls the strength of the

attraction. The attraction moves parameters towards the center of the trajectory or bottom of the valley (Figure 1b). In principle, we can make γ negative and have repulsive forces, which is not of interest in this paper. We add weight decay with a similar method as AdamW (Loshchilov & Hutter, 2019) and ω is the vector encoding weight decay (not all parameters have non-zero weight decay).

We next study the performance of FOCUS on our toy landscapes. We follow the same procedure to find the best performance over different learning rates of FOCUS ($\gamma = 0.2$) as Adam and Signum in Figure 2. We use the blue region to denote the conditions where FOCUS is the best optimizer. We find that FOCUS outperforms Signum when sharpness is large with high probability (Figure 2a). The checkered pattern between blue and yellow suggests that FOCUS and Signum reach similar depths, but FOCUS appears more stable staying deep in the valley. FOCUS cannot be better than Signum if weight decay is too large (Figure 2b). A large weight decay helps Signum to stay close to the bottom of the valley and the attraction force no longer has an advantage. However, FOCUS does not outperform Adam more than Signum did as the boundary between Adam and FOCUS is almost the same as that between Adam and Signum (Figure 2, a and b). We conclude that FOCUS is an improved Signum that can outperform Adam when the effect of gradient noise is larger than that of sharpness.

3. Experiments

3.1. Setup

Now, we are ready to evaluate whether our insights and proposed optimizer can contribute to LLM pre-training. We train a small GPT-2 model with 125 million parameters (Radford et al., 2019; Liu et al., 2023a) on OpenWebText (Gokaslan & Cohen, 2019). Detailed model configuration can be found in Appendix A.3.

We use the optimal performance of Adam (more precisely, AdamW (Loshchilov & Hutter, 2019)) scanned over hyperparameters in Liu et al. (2023a) as our baseline for comparison. Due to our limited computing resources, we cannot scan optimal performance for FOCUS systematically on GPT-2 training. For FOCUS, some hyperparameters around Adam’s optimal choice, learning rate 6×10^{-4} , $\beta_1 = 0.9$, $\beta_2 = 0.95$, and weight decay 0.1, are tested. The idea is that if there exists any performance of FOCUS better than the best performance of Adam, the best performance of FOCUS is certainly better than that of Adam.

Our code implementation adopts those in Liu et al. (2023a) to eight V100 GPUs with `float16`. We use a batch size of 480. The learning rate is subject to a warm-up lasting two thousand steps and then a cosine schedule decreasing it to a final value around 0.05 times the peak learning rate

(Rae et al., 2021). If not specified, “learning rate” in this section refers to the peak learning rate. A standard gradient clipping (by norm) is used with a threshold of 1.0.

In the following, we show our results of GPT-2 training and compare them to our intuition from toy model experiments.

3.2. Stability

Recall that FOCUS improves Signum when facing a sharp landscape with large gradient noise. We compare FOCUS ($\gamma = 0.2$, $\beta_1 = 0.9$, $\beta_2 = 0.99$, weight decay 0.2) with Signum (i.e., FOCUS having $\gamma = 0$, $\beta_1 = 0.9$, $\beta_2 = 0$, and weight decay 0.2). With the same learning rate 6×10^{-4} and the number of training steps 10^5 , we find FOCUS is slower than Signum at the early stages. If actual parameters are “ahead” of the EMA of parameters, attraction force effectively decreases the step size from 1 to $1 - \gamma$. However, Signum rapidly becomes unstable (Figure 3a). We then decrease the learning rate to 10^{-4} for Signum, yet still cannot obtain a stable training process. And at a learning rate 10^{-4} , Signum is already slower than FOCUS. In training GPT-2, FOCUS outperforms Signum because FOCUS is much more stable and picks much larger learning rates.

We next compare FOCUS with Adam on our machines. We find the optimal hyperparameters reported in Liu et al. (2023a) for Adam (i.e., learning rate 6×10^{-4} , $\beta_1 = 0.9$, $\beta_2 = 0.95$, and weight decay 0.1) lead to unstable training on V100 GPUs with `float16` (Figure 3b). We doubled the weight decay but did not obtain stable training (see Appendix B). Then, we decrease the learning rate to 3×10^{-4} and 10^{-4} . Finally, Adam becomes stable at a learning rate 10^{-4} but yields much slower training and higher final validation loss than FOCUS (Figure 3b). We conclude that FOCUS is more stable than Adam in `float16`.

3.3. Speedup

So far, we can claim FOCUS gains speedup compared to Signum and Adam on the machines we use. However, the speedup is mainly due to stability issues of other algorithms which may not be a problem on better machines or floating-point format (e.g., `bfloat16`) that are used widely.

To see whether FOCUS can have a more relevant speedup, we compare FOCUS with the optimal performance of Adam in Liu et al. (2023a). Adam is stable with a large learning rate 6×10^{-4} possibly due to the use of `bfloat16`. We observe that given the same training steps (i.e., 10^5), one training case of FOCUS reaches a lower final loss than the optimal Adam reported in Liu et al. (2023a) (Figure 3c). If we decrease the training steps of FOCUS, which makes the scheduler decrease learning rate faster (the final learning rate remains the same), we find that FOCUS approximately achieves a twice speedup: the loss of FOCUS running $5 \times$

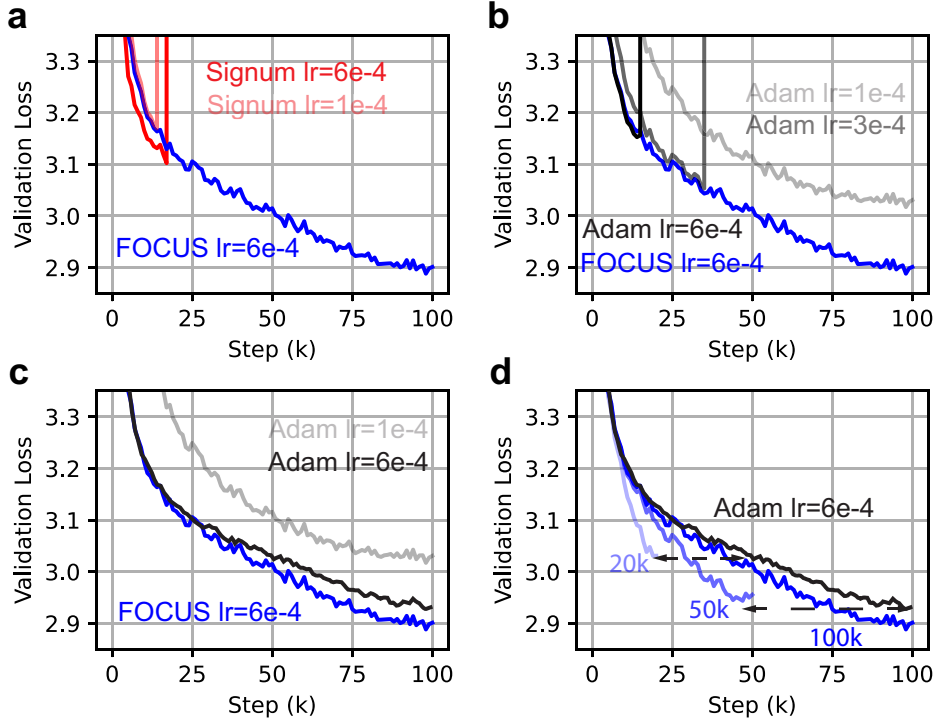


Figure 3. FOCUS is more stable and faster in training GPT-2 (small). (a) In `float16` and with the same hyperparameters, FOCUS is slower than Signum, but Signum is unstable. The smaller learning rate of Signum leads to slower training than FOCUS yet is still unstable. (b) Similarly, in `float16`, FOCUS is more stable than Adam and stable Adam training is much slower. (c) We copy the optimal performance of Adam (trained in `bfloat16`) from Liu et al. (2023a) (black line), which is still slower than our FOCUS. (d) Decreasing the number of training steps of FOCUS (which also changes the learning rate scheduler), we find FOCUS can achieve a 2x speedup compared to Adam. More details in Appendix A.

10^4 steps is close to that of Adam running 10^5 steps and the loss of FOCUS running 2×10^4 steps is close to that of Adam running 5×10^4 steps (Figure 3d). Even though Adam can avoid instability issues via other techniques, FOCUS can still outperform Adam.

To conclude, our FOCUS optimizer, which aims to improve Signum to better handle sharpness and to avoid decreasing effective step size too much like Adam when gradient stochasticity is large, gains practical speedup in training GPT-2 compared to Adam. According to our toy model, this result suggests that LLM training has relatively large gradient noises, which may be a key limiting factor in training and needs more attention in future studies.

4. Convergence analysis

As a sanity check, we analyze the worst-case convergence rate of FOCUS in the online convex optimization framework (Zinkevich, 2003; Kingma & Ba, 2014). We consider the optimization of a sequence of convex loss functions $\{L_t\}_{t=1}^T$ over a convex set $\mathcal{F} \subseteq \mathbb{R}^d$.

Definition 4.1 (Online Optimization Protocol). At each time step t : (1) The optimizer goes to parameters $\theta_t \in \mathcal{F}$; (2) The loss function L_t is revealed; (3) The optimizer incurs loss $L_t(\theta_t)$ and observes gradient $g_t = \nabla L_t(\theta_t)$.

The algorithm is evaluated via regret since the sequence is unknown in advance (Zinkevich, 2003). The regret after T iterations is

$$R(T) = \sum_{t=1}^T [L_t(\theta_t) - L_t(\theta^*)], \quad (5)$$

where $\theta^* = \arg \min_{\theta \in \mathcal{F}} \sum_{t=1}^T L_t(\theta)$.

Our analysis shows that FOCUS has a regret bound $O(\sqrt{T})$ which is the same as Adam in terms of dependence on the order of T (Kingma & Ba, 2014). In other words, the mean regret $R(T)/T$ converges as $O(1/\sqrt{T})$. The result is stated formally below and the proof is in Appendix C.

Theorem 4.2 (Regret Bound). Let $\{L_t\}_{t=1}^T$ be a sequence of convex functions with bounded gradients $\|g_t\|_\infty \leq G_\infty$. For the FOCUS optimizer with learning rate $\eta_t = \eta/\sqrt{t}$,

$\beta_1, \beta_2 \in [0, 1)$, $\beta_{1,t} = \beta_1 \lambda_\beta^t$, $\gamma_t = \gamma \lambda_\gamma^t$,¹ and $\lambda_\beta, \lambda_\gamma \in [0, 1)$, assuming the distance between any two points in \mathcal{F} are bounded in infinity norm by D_∞ and in 2-norm by D , the regret is bounded by:

$$R(T) \leq \frac{G_\infty(D^2 + dD_\infty^2\sqrt{T})}{2\eta(1 - \beta_1)} + \frac{G_\infty\eta d\sqrt{T}}{(1 - \beta_1)}(1 + |\gamma|)^2 + \left(\frac{\beta_1\lambda_\beta d}{1 - \lambda_\beta} + \frac{|\gamma|\lambda_\gamma d}{1 - \lambda_\gamma}\right) \frac{G_\infty D_\infty}{1 - \beta_1} \quad (6)$$

Theoretically, decaying $\beta_{1,t}$ and γ_t are important to bound some summation terms in $R(T)$. However, those summation terms may be small themselves and do not need decaying $\beta_{1,t}$ or γ_t . The worst-case analysis does not reflect the advantage of introducing momentum or attraction and has limited insights into designing new algorithms. On the other hand, it is still interesting to study the effect of decaying force. For a sanity check, we conclude that FOCUS can achieve the same convergence rate as Adam on the same online convex optimization problem.

5. Related works

Valley-like loss landscapes Although strongly convex loss landscapes are easier to analyze, empirical evidence has shown that loss landscapes are usually valley-like: [Sagun et al. \(2016\)](#) found that eigenvalues of Hessians are split into the bulk part concentrated around zero and the edge part away from zero. The large eigenvalues correspond to directions with fast loss changes, while the near-zero eigenvalues correspond to the relatively flat regions at the bottom of the valley. This valley picture also agrees with the observation that gradient descent happens mostly in a tiny subspace ([Gur-Ari et al., 2018](#)). Like our paper, research has looked into the role of noise in valley-like landscapes ([Wei & Schwab, 2019](#)), suggesting that the noise drifts the parameter towards a less sharp landscape. Although noise in SGD was deemed beneficial in earlier works ([Kleinberg et al., 2018](#); [Chaudhari et al., 2019](#)), since they can help escape local minima and find flatter (hence more generalizable) solutions, recent work in large language models suggests that noise is the enemy. [Wen et al. \(2024\)](#) recently revisits the valley loss landscape in the context of language models, suggesting that noise or large learning rates prevent the optimizer from getting to the bottom of the valley. The main idea of FOCUS agrees with this picture: a good optimizer for LLMs should be able to squeeze into a sharp valley.

Optimizers Despite the family of adaptive optimizers (Adam, Adagrad) dominating the deep learning world, there are newly proposed optimizers that are shown to demonstrate superior performance for language model pretrain-

¹We generalize the optimizer to have a time-dependent decay rate, i.e., $\beta_{1,t}$, and a time-dependent force strength, i.e., γ_t .

ing. These methods include Lion ([Chen et al., 2024](#)), AdEMAMix ([Pagliardini et al., 2024](#)), MARS ([Yuan et al., 2024](#)), cautious optimizers ([Liang et al., 2024](#)), modular optimizers ([Large et al., 2024](#)), Sophia ([Liu et al., 2023a](#)), soap ([Vyas et al., 2024](#)) (combining Adam with Shampoo ([Gupta et al., 2018](#))), muon ([Jordan et al., 2024](#)), Adam-mini ([Zhang et al., 2024](#)), etc. These optimizers are mostly mathematics-inspired, while FOCUS is physics-inspired (self-attracting gas). Our analysis also involves physical tools like phase diagrams which illuminate when Adam/Signum is more performant than the other, providing insights into the question of why Signum works at all ([Bernstein et al., 2018](#); [Large et al., 2024](#)), and that Adam is not always better than Signum ([Zhao et al., 2024](#)).

Weight averaging The EMA of a training trajectory has been used to obtain model parameters with better prediction stability and generalizability ([Grill et al., 2020](#); [He et al., 2020](#); [Morales Brotons et al., 2024](#)). However, we use the EMA of parameters to modify the optimizer and change training dynamics directly.

6. Discussion

We discuss our physics picture Figure 1b in physics language. For a stochastic optimization process, the optimizer should end up being at the minimum of free energy

$$F = E - \Theta S, \quad (7)$$

where energy E is the loss value, Θ is temperature related to batch size, learning rate, etc., and S is entropy. Squeezing in the narrowing valley, the effective volume of the “bouncing particles” is decreasing so that S is decaying which tends to increase F . At some point, when the energetic force (i.e., gradient) balances the entropic force, the optimizer is stuck. We introduce attraction force which effectively adds a term to energy that prefers small volumes, fighting against the decaying entropy.

The mechanistic reasons behind LLM having sharp valley landscapes and large gradient stochasticity may be the same—large uncertainty in data distribution ([Wen et al., 2024](#)). Language is special in having such a large variability, diversity, and richness, giving rise to unique training dynamics. FOCUS outperforms Adam in our GPT-2 training (Section 3) because the batch size may still be small given the language task and dataset. Yet, how large the batch size we need for LLM to have a small gradient noise is an open question.

The fact that FOCUS can be faster indicates large gradient noise is an important limiting factor in training LLMs. According to FOCUS’s ability to deal with large noises and instabilities, we suggest trying it with limited batch sizes, low-precision training, etc. Future research is needed to fully explore the utility of FOCUS and our physical picture.

Acknowledgements

Y. L. thanks Tongyang Li for helpful suggestions.

References

- Andriushchenko, M., D’Angelo, F., Varre, A., and Flammarion, N. Why do we need weight decay in modern deep learning?, 2024. URL <https://openreview.net/forum?id=RKh7DI23tz>.
- Bernstein, J., Wang, Y.-X., Azizadenesheli, K., and Anandkumar, A. sigsgd: Compressed optimisation for non-convex problems. In *International Conference on Machine Learning*, pp. 560–569. PMLR, 2018.
- Brown, T. B., Mann, B., Ryder, N., Subbiah, M., Kaplan, J., Dhariwal, P., Neelakantan, A., et al. Language models are few-shot learners. *Advances in Neural Information Processing Systems*, 33:1877–1901, 2020.
- Chaudhari, P., Choromanska, A., Soatto, S., LeCun, Y., Baldassi, C., Borgs, C., Chayes, J., Sagun, L., and Zecchina, R. Entropy-sgd: Biasing gradient descent into wide valleys. *Journal of Statistical Mechanics: Theory and Experiment*, 2019(12):124018, 2019.
- Chen, M., Tworek, J., Jun, H., Yuan, Q., et al. Evaluating large language models trained on code. *arXiv preprint arXiv:2107.03374*, 2021. <https://arxiv.org/abs/2107.03374>.
- Chen, X., Liang, C., Huang, D., Real, E., Wang, K., Pham, H., Dong, X., Luong, T., Hsieh, C.-J., Lu, Y., et al. Symbolic discovery of optimization algorithms. *Advances in neural information processing systems*, 36, 2024.
- GitHub. Github copilot: Your ai pair programmer, 2022. <https://github.com/features/copilot>.
- Gokaslan, A. and Cohen, V. Openwebtext corpus, 2019.
- Grill, J.-B., Strub, F., Altché, F., Tallec, C., Richemond, P. H., Buchatskaya, E., Doersch, C., Pires, B. A., Guo, Z. D., Azar, M. G., Piot, B., Kavukcuoglu, K., Munos, R., and Valko, M. Bootstrap your own latent: A new approach to self-supervised learning, 2020. URL <https://arxiv.org/abs/2006.07733>.
- Gupta, V., Koren, T., and Singer, Y. Shampoo: Pre-conditioned stochastic tensor optimization. In *International Conference on Machine Learning*, pp. 1842–1850. PMLR, 2018.
- Gur-Ari, G., Roberts, D. A., and Dyer, E. Gradient descent happens in a tiny subspace. *arXiv preprint arXiv:1812.04754*, 2018.
- He, K., Fan, H., Wu, Y., Xie, S., and Girshick, R. Momentum contrast for unsupervised visual representation learning. In *Proceedings of the IEEE/CVF Conference on Computer Vision and Pattern Recognition (CVPR)*, June 2020.
- Hoffmann, J., Borgeaud, S., Mensch, A., Rae, J. W., Lai, A., Wang, J., Millican, K., Young, S., Tieleman, O., et al. Training compute-optimal large language models. *arXiv preprint arXiv:2203.15556*, 2022.
- Jin, H., Wei, W., Wang, X., Zhang, W., and Wu, Y. Rethinking learning rate tuning in the era of large language models, 2023. URL <https://arxiv.org/abs/2309.08859>.
- Jordan, K., Jin, Y., Boza, V., Jiacheng, Y., Cecista, F., Newhouse, L., and Bernstein, J. Muon: An optimizer for hidden layers in neural networks, 2024. URL <https://kellerjordan.github.io/posts/muon/>.
- Kaplan, J., McCandlish, S., Henighan, T., Brown, T. B., Chess, B., Child, R., Gray, S., Radford, A., Wu, J., and Amodei, D. Scaling laws for neural language models. *arXiv preprint arXiv:2001.08361*, 2020.
- Kingma, D. P. and Ba, J. Adam: A method for stochastic optimization. *arXiv preprint arXiv:1412.6980*, 2014.
- Kleinberg, B., Li, Y., and Yuan, Y. An alternative view: When does sgd escape local minima? In *International conference on machine learning*, pp. 2698–2707. PMLR, 2018.
- Large, T., Liu, Y., Huh, M., Bahng, H., Isola, P., and Bernstein, J. Scalable optimization in the modular norm. *arXiv preprint arXiv:2405.14813*, 2024.
- LeCun, Y., Cortes, C., and Burges, C. J. The MNIST database of handwritten digits. <http://yann.lecun.com/exdb/mnist/>, 1998.
- Lewkowycz, A., Minervini, P., Andreas, J., et al. Solving quantitative reasoning problems with language models. *arXiv preprint arXiv:2206.14858*, 2022. <https://arxiv.org/abs/2206.14858>.
- Liang, K., Chen, L., Liu, B., and Liu, Q. Cautious optimizers: Improving training with one line of code. *arXiv preprint arXiv:2411.16085*, 2024.
- Liu, H., Li, Z., Hall, D., Liang, P., and Ma, T. Sophia: A scalable stochastic second-order optimizer for language model pre-training. *arXiv preprint arXiv:2305.14342*, 2023a.
- Liu, Y. Complex fractal trainability boundary can arise from trivial non-convexity, 2024. URL <https://arxiv.org/abs/2406.13971>.

- Liu, Y., Su, W. J., and Li, T. On Quantum Speedups for Nonconvex Optimization via Quantum Tunneling Walks. *Quantum*, 7:1030, June 2023b. ISSN 2521-327X. doi: 10.22331/q-2023-06-02-1030. URL <https://doi.org/10.22331/q-2023-06-02-1030>.
- Loshchilov, I. and Hutter, F. Sgdr: Stochastic gradient descent with warm restarts, 2017. URL <https://arxiv.org/abs/1608.03983>.
- Loshchilov, I. and Hutter, F. Decoupled weight decay regularization. In *International Conference on Learning Representations*, 2019. URL <https://openreview.net/forum?id=Bkg6RiCqY7>.
- Morales Brotons, D., Vogels, T., and Hendriks, H. Exponential Moving Average of Weights in Deep Learning: Dynamics and Benefits. *Transactions on Machine Learning Research Journal*, pp. 1–27, April 2024. URL <https://hal.science/hal-04830859>.
- OpenAI. Gpt-4 technical report, 2023. <https://openai.com/research/gpt-4>.
- Pagliardini, M., Ablin, P., and Grangier, D. The adamix optimizer: Better, faster, older. *arXiv preprint arXiv:2409.03137*, 2024.
- Qin, H., Ji, G.-P., Khan, S., Fan, D.-P., Khan, F. S., and Van Gool, L. How good is google bard’s visual understanding? an empirical study on open challenges. *arXiv preprint arXiv:2307.15016*, 2023. <https://arxiv.org/abs/2307.15016>.
- Radford, A., Wu, J., Child, R., Luan, D., Amodei, D., Sutskever, I., et al. Language models are unsupervised multitask learners. *OpenAI blog*, 1(8):9, 2019.
- Rae, J. W., Borgeaud, S., Cai, T., et al. Scaling language models: Methods, analysis & insights from training gopher. *arXiv preprint arXiv:2112.11446*, 2021. <https://arxiv.org/abs/2112.11446>.
- Sagun, L., Bottou, L., and LeCun, Y. Eigenvalues of the hessian in deep learning: Singularity and beyond. *arXiv preprint arXiv:1611.07476*, 2016.
- Shi, B., Su, W. J., and Jordan, M. I. On learning rates and schrödinger operators, 2020. URL <https://arxiv.org/abs/2004.06977>.
- Sohl-Dickstein, J. The boundary of neural network trainability is fractal, 2024. URL <https://arxiv.org/abs/2402.06184>.
- Subramanian, S., Ganapathiraman, V., and Barrett, C. Hop, skip, jump to convergence: Dynamics of learning rate transitions for improved training of large language models, 2024.
- Taylor, R., Kardas, M., Cucurull, G., Scialom, T., Hartshorn, A., Saravia, E., Poulton, A., et al. Galactica: A large language model for science. *arXiv preprint arXiv:2211.09085*, 2022. <https://arxiv.org/abs/2211.09085>.
- Trinh, T. H., Wu, Y., Le, Q. V., He, H., and Luong, T. Solving olympiad geometry without human demonstrations. *Nature*, 2024. <https://www.nature.com/articles/s41586-024-00001-2>.
- Vyas, N., Morwani, D., Zhao, R., Shapira, I., Brandfonbrener, D., Janson, L., and Kakade, S. Soap: Improving and stabilizing shampoo using adam. *arXiv preprint arXiv:2409.11321*, 2024.
- Wang, X. and Aitchison, L. How to set adamw’s weight decay as you scale model and dataset size, 2024. URL <https://arxiv.org/abs/2405.13698>.
- Wei, M. and Schwab, D. J. How noise affects the hessian spectrum in overparameterized neural networks. *arXiv preprint arXiv:1910.00195*, 2019.
- Wen, K., Li, Z., Wang, J., Hall, D., Liang, P., and Ma, T. Understanding warmup-stable-decay learning rates: A river valley loss landscape perspective. *arXiv preprint arXiv:2410.05192*, 2024.
- Wolfram, S. Wolfram—alpha as the computation engine for gpt models, 2023. <https://www.wolfram.com/wolfram-alpha-openai-plugin>.
- Yuan, H., Liu, Y., Wu, S., Zhou, X., and Gu, Q. Mars: Unleashing the power of variance reduction for training large models. *arXiv preprint arXiv:2411.10438*, 2024.
- Zhang, Y., Chen, C., Li, Z., Ding, T., Wu, C., Kingma, D. P., Ye, Y., Luo, Z.-Q., and Sun, R. Adam-mini: Use fewer learning rates to gain more, 2024. URL <https://arxiv.org/abs/2406.16793>.
- Zhao, R., Morwani, D., Brandfonbrener, D., Vyas, N., and Kakade, S. Deconstructing what makes a good optimizer for language models. *arXiv preprint arXiv:2407.07972*, 2024.
- Zinkevich, M. Online convex programming and generalized infinitesimal gradient ascent. In *Proceedings of the 20th international conference on machine learning (icml-03)*, pp. 928–936, 2003.

A. Model details

A.1. Toy model

The experiment utilizes a two-dimensional optimization landscape defined by the function Equation (1) where u represents the coordinates after rotation by $\theta = \pi/6$ radians (30 degrees). The landscape parameters are set to $a = 10$ and $c = 0.1$. The rotation is implemented using a standard 2D rotation matrix:

$$\begin{pmatrix} \cos(\theta) & -\sin(\theta) \\ \sin(\theta) & \cos(\theta) \end{pmatrix} \quad (8)$$

The experiment compares three optimization configurations:

1. Adam optimizer with $\beta_1 = 0.9$, $\beta_2 = 0.999$
2. FOCUS optimizer with $\beta_1 = 0.9$, $\beta_2 = 0.9$, $\gamma = 0.2$
3. Signum optimizer with $\beta_1 = 0.9$

The experiment shown in Figure 2a systematically explores the following parameter ranges:

- Landscape sharpness (a): 96 values logarithmically spaced between 10^{-1} and 10^3
- Noise standard deviation: 100 values linearly spaced between 0 and 3
- Learning rates: 20 values logarithmically spaced between 10^{-3} and 10^0

Each configuration was tested with 50 independent replicates. For each replicate:

- Initial positions were randomly initialized with standard deviation 10^{-4}
- Optimization proceeded for 1000 steps
- Weight decay was fixed at 0.1 across all experiments
- The final loss value was recorded for analysis

The implementation includes several important technical considerations:

- Gradient computation incorporates multiplicative noise with a controlled standard deviation
- Adam uses $\epsilon = 10^{-8}$ for numerical stability in its denominator
- Momentum-based bias correction is applied for both optimizers

Results are stored in a 6-dimensional array with the following dimensions:

- 3 (optimizer configurations)
- 100 (noise levels)
- 96 (sharpness)
- 20 (learning rates)
- 50 (replicates)
- 1 (metrics: final loss)

Results for each landscape sharpness configuration are saved as separate numpy arrays, with filenames indicating the corresponding task ID in the format `syn-exp-7-{task_id}.npz`.

In Figure 2b, we do the following to obtain the $96 \text{ pixel} \times 100 \text{ pixel}$ phase diagram. For each optimizer configuration, the following parameters were systematically varied:

- Learning rates: 20 values logarithmically spaced between 10^{-3} and 10^0
- Noise standard deviation: 100 values linearly spaced between 0 and 3
- Weight decay: 96 values linearly spaced between 0 and 0.5

Each configuration was tested with 50 independent replicates. For each replicate:

- Initial positions were randomly initialized with standard deviation 10^{-4}
- Optimization proceeded for 1000 steps
- Three metrics were tracked:
 1. Final loss value
 2. Historical minimum loss achieved
 3. Projection onto the valley axis (defined by rotation angle $\pi/6$)

The implementation includes several important technical considerations:

- Gradient computation incorporates multiplicative noise with a controlled standard deviation
- Weight decay is implemented as an additive term in parameter updates
- Adam uses $\epsilon = 10^{-8}$ for numerical stability in its denominator
- Momentum-based bias correction is applied for both optimizers

The final results can be put in a 6-dimensional array with the following dimensions:

- 3 (optimizer configurations)
- 100 (noise levels σ)
- 96 (weight decay)
- 20 (learning rates)
- 50 (replicates)
- 3 (metrics: final loss, minimum loss along the trajectory, valley projection)

Results for each weight decay configuration are saved as separate numpy arrays, with filenames indicating the corresponding task ID in the format `syn-exp-6-{task_id}.npz`.

A.2. MLP

The experiment in Figure 2 c and d employs a multi-layer perceptron (MLP) with the following architecture:

- Input dimension: 784 (flattened MNIST images)
- Five hidden layers of 128 units each
- Output dimension: 10 (number of MNIST classes)
- ReLU activation functions between layers
- Batch normalization applied before each linear layer

The MNIST dataset was used with the following specifications:

- Images resized to 28×28 pixels
- Pixel values normalized to $[0,1]$ through ToTensor transformation
- Training set: 60,000 images
- Test set: 10,000 images
- Test batch size fixed at 8,192 samples

The experiment compares four optimization configurations:

1. AdamW with standard parameters ($\beta_1 = 0.9$, $\beta_2 = 0.999$)
2. Signum with $\beta_1 = 0.9$
3. FOCUS with $\beta_1 = 0.9$, $\beta_2 = 0.99$, $\gamma = 0.2$
4. FOCUS with $\beta_1 = 0.9$, $\beta_2 = 0.99$, $\gamma = 0.4$

The experiment systematically explores the following parameter ranges:

- Learning rates: 20 values logarithmically spaced between 10^{-4} and 10^0
- Batch sizes: 12 values as powers of 2, ranging from 2^1 to 2^{12}
- Weight decay: Fixed at 10^{-2} for all experiments

Each configuration was tested with three independent replicates. For each replicate:

- Training proceeded for 400 steps
- Cross-entropy loss was used as the optimization objective
- Weight decay was selectively applied (excluded for bias and batch normalization parameters)
- Training loss, test loss, and test accuracy were recorded at each step

Several technical considerations were incorporated:

- Gradient computations used PyTorch’s autograd system
- Data loading utilized pin_memory for improved GPU transfer efficiency

- Parameters were separated into two groups for differential weight decay application
- Test evaluation was performed with `torch.no_grad()` for memory efficiency

All results are stored in a 5-dimensional tensor with the following dimensions:

- 12 (batch sizes)
- 20 (learning rates)
- 3 (replicates)
- 400 (training steps)
- 3 (metrics: training loss, test loss, test accuracy)

Results for each combination of optimizer type and batch size are saved as separate PyTorch tensors, with filenames indicating the corresponding task ID in the format `scan-18-{task_id}.pt`.

A.3. GPT-2

We implement the GPT-2 small architecture with 125M parameters as described in Radford et al. (2019) which has embedding dimension 768, number of heads 12, and number of layers 12. We use Liu et al. (2023a) codebase as our implementation foundation which is based on nanoGPT (<https://github.com/karpathy/nanoGPT/>). Following nanoGPT’s architecture choices, we use GELU activations and disable bias and Dropout during pre-training.

Our model is trained on OpenWebText (Gokaslan & Cohen, 2019). The text is tokenized using the standard GPT-2 tokenizer (Radford et al., 2019). We utilize the train and validation split provided by nanoGPT, where the training set contains 9B tokens and the validation set contains 4.4M tokens.

To enable efficient training, we implement distributed data parallel (DDP) training across 8 NVIDIA V100 GPUs with gradient accumulation to maintain an effective batch size of 480 ($480 = 12 \times 5 \times 8$, where 12 is the batch size on each GPU, 5 is the number of gradient accumulation steps, and 8 is the number of GPUs). The entire training process is conducted using `float16` precision to optimize memory usage and computational efficiency.

Figure 3a compares three optimization configurations:

1. Signum with learning rate 6×10^{-4} , $\beta_1 = 0.9$, weight decay 0.2, 10^5 training steps
2. Signum with learning rate 10^{-4} , $\beta_1 = 0.9$, weight decay 0.2, 10^5 training steps
3. FOCUS with learning rate 6×10^{-4} , $\beta_1 = 0.9$, $\beta_2 = 0.99$, $\gamma = 0.2$, weight decay 0.2, 10^5 training steps

Figure 3b compares four optimization configurations:

1. Adam with learning rate 6×10^{-4} , $\beta_1 = 0.9$, $\beta_2 = 0.95$, weight decay 0.1, 10^5 training steps
2. Adam with learning rate 3×10^{-4} , $\beta_1 = 0.9$, $\beta_2 = 0.95$, weight decay 0.1, 10^5 training steps
3. Adam with learning rate 10^{-4} , $\beta_1 = 0.9$, $\beta_2 = 0.95$, weight decay 0.1, 10^5 training steps
4. FOCUS with learning rate 6×10^{-4} , $\beta_1 = 0.9$, $\beta_2 = 0.99$, $\gamma = 0.2$, weight decay 0.2, 10^5 training steps

Figure 3c compares three optimization configurations:

1. Adam with learning rate 6×10^{-4} , $\beta_1 = 0.9$, $\beta_2 = 0.95$, weight decay 0.1, 10^5 training steps (result copied from Liu et al. (2023a))
2. Adam with learning rate 10^{-4} , $\beta_1 = 0.9$, $\beta_2 = 0.95$, weight decay 0.1, 10^5 training steps

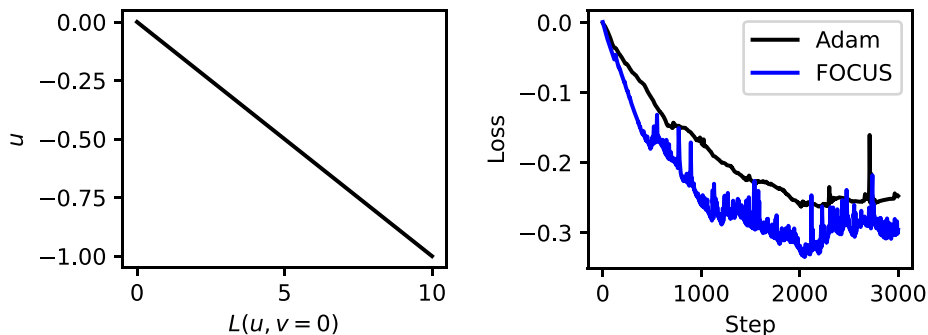


Figure 4. Training dynamics reaches steady state on the narrowing valley. The left panel is $L(u, v = 0) = -cu$ showing our toy landscape can go to negative infinity ($c = 0.1$ in this case). The right panel is the loss for Adam (learning rate 0.005, $\beta_1 = 0.9$, $\beta_2 = 0.999$, weight decay 0.1) and FOCUS (learning rate 0.005, $\beta_1 = 0.9$, $\beta_2 = 0.9$, $\gamma = 0.2$, weight decay 0.1) on the toy landscape with $a = 10$ and $c = 0.1$. Both training dynamics already converge within 3000 steps.

3. FOCUS with learning rate 6×10^{-4} , $\beta_1 = 0.9$, $\beta_2 = 0.99$, $\gamma = 0.2$, weight decay 0.2, 10^5 training steps

Figure 3d compares four optimization configurations:

1. Adam with learning rate 6×10^{-4} , $\beta_1 = 0.9$, $\beta_2 = 0.95$, weight decay 0.1, 10^5 training steps (result copied from Liu et al. (2023a))
2. FOCUS with learning rate 6×10^{-4} , $\beta_1 = 0.9$, $\beta_2 = 0.99$, $\gamma = 0.2$, weight decay 0.2, 10^5 training steps
3. FOCUS with learning rate 6×10^{-4} , $\beta_1 = 0.9$, $\beta_2 = 0.99$, $\gamma = 0.2$, weight decay 0.2, 5×10^4 training steps
4. FOCUS with learning rate 10^{-3} , $\beta_1 = 0.9$, $\beta_2 = 0.99$, $\gamma = 0.2$, weight decay 0.2, 2×10^4 training steps

B. Supplementary results

The landscape we construct can go to negative infinity (see Figure 4 right panel) which is unrealistic. Our construction serves as a good local approximation. Despite the unrealistic part, we emphasize the key takeaway that because the valley is narrowing, the positions that can be reached with finite learning rates are far from the true minimum ($-\infty$ in our construction but 0 in real cases). We also discuss this phenomenon through the balance between the gradient (energetic term) and an “entropic” term associated with finite learning rate and gradient stochasticity (see Section 6). In practice, with non-zero weight decay, the optimizer can go along one parameter bounded by the inverse weight decay. However, the true parameter values the optimizers stay at (in Figure 4 right panel, parameters are around $2 \sim 3$) are much smaller than the inverse weight decay (which is 10 in Figure 4, the right panel). If the narrowing valley picture is true, we meet a problem for all optimizers similar to Zeno’s paradox: we need a smaller learning rate to go deeper into the valley, but a smaller learning rate reduces the speed moving along the valley. The narrowing valley makes the optimizer stay at a place far from the true optimum in the valley, which provides another perspective for the neural scaling laws (Kaplan et al., 2020; Hoffmann et al., 2022): the scaling laws may be due to training dynamics rather than the limit of the model.

In Figure 5, we provide detailed pair comparisons between optimizers based on the same data as Figure 2 a and b, which shows more details. As stated in the main text, the checkered pattern between blue and yellow may suggest that FOCUS does not reach significantly deeper in the valley but may be more stable such that with high probability we can see blue in the mixed region. We tend to interpret this checkered pattern through stochasticity rather than sensitivity to hyperparameters in deterministic training setup (Sohl-Dickstein, 2024; Liu, 2024). We also tune and generalize our toy landscapes which gives the same qualitative results (Figure 6). For GPT-2 training, we find that increasing weight decay does not suffice to stabilize Adam (Figure 7), and therefore we decrease the learning rate in the main text to try to obtain stable training on our machines. We also find that FOCUS needs a longer time to finish the same number of steps while the extra time is negligibly small (Figure 8). Since in terms of the algorithms, FOCUS is not more complex than Adam nor requires more memory, we

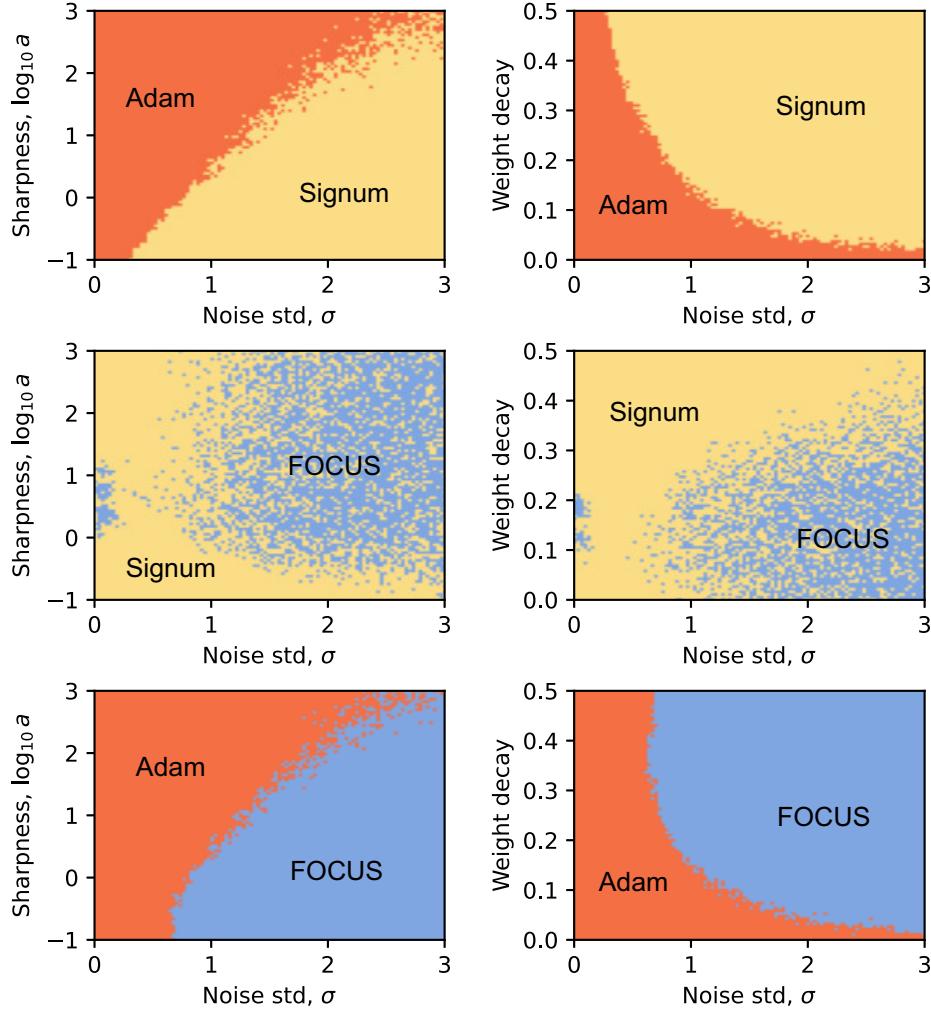


Figure 5. Pairwise comparisons between optimizers. This figure uses the same data as Figure 2, a and b. We plot all the pairwise comparisons, showing more details to support the conclusion.

hypothesize that this extra time is due to our unsophisticated code implementation of FOCUS which has some room for improvement.

C. Convergence proof

Lemma C.1 (Convex function). *If a function f over \mathbb{R}^d is convex, then for all $x, y \in \mathbb{R}^d$,*

$$f(y) \geq f(x) + \langle \nabla f(x), y - x \rangle. \quad (9)$$

The above lemma is a standard property of convex functions.

Lemma C.2 (Momentum bound). *Let $m_{t,i}$ be the i th element of momentum vector m_t , g_t is the gradient obtained at step t satisfying $\|g_t\|_\infty \leq G_\infty$, and $m_t = \beta_{1,t}m_{t-1} + (1 - \beta_{1,t})g_t$ with $\beta_{1,t} \in [0, 1)$, we have $|m_{t,i}| \leq G_\infty$ for all t and i .*

Proof. First of all, $|m_0| = 0 \leq G_\infty$. We next assume that $|m_{t-1,i}| \leq G_\infty$ for all i . Then, $|m_{t,i}| = |\beta_{1,t}m_{t-1,i} + (1 - \beta_{1,t})g_{t,i}| \leq |\beta_{1,t}m_{t-1,i}| + |(1 - \beta_{1,t})g_{t,i}| \leq \beta_{1,t}G_\infty + (1 - \beta_{1,t})G_\infty = G_\infty$. According to mathematical induction, the proof is completed. \square

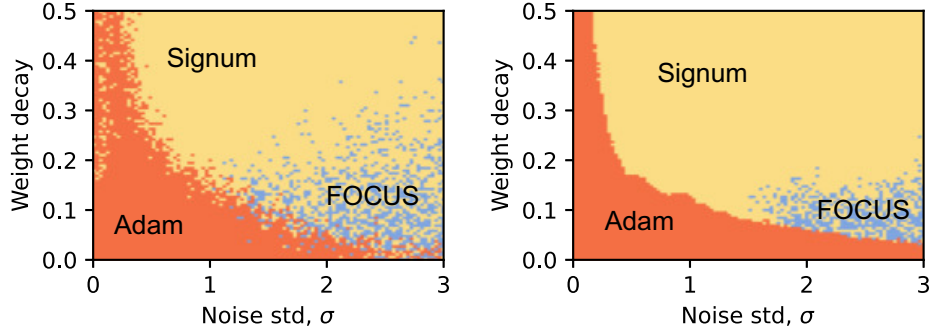


Figure 6. Toy landscape can have various forms and our results hold qualitatively and robustly. The left panel is obtained following the same procedure as Figure 2b described in Appendix A.1 but with u being x (i.e., no rotation). To obtain the right panel, we generalize the toy landscape to be high-dimensional (100 dimensions). The idea is to expand v into a vector and the resulting landscape has axial symmetry along u . The u, v coordinate is obtained by a random rotation from the parameter directions first.

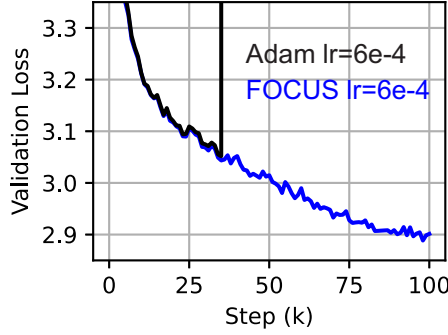


Figure 7. Increasing the weight decay cannot stabilize Adam. The black line here is Adam with learning rate 6×10^{-4} , $\beta_1 = 0.9$, $\beta_2 = 0.95$, weight decay 0.2, and 10^5 training steps. The blue line is the same as Figure 3.

Theorem C.3 (Regret Bound). Let $\{L_t\}_{t=1}^T$ be a sequence of convex functions with bounded gradients $\|g_t\|_\infty \leq G_\infty$. For the FOCUS optimizer with learning rate $\eta_t = \eta/\sqrt{t}$, $\beta_1, \beta_2 \in [0, 1)$, $\beta_{1,t} = \beta_1 \lambda_\beta^t$, $\gamma_t = \gamma \lambda_\gamma^t$, and $\lambda_\beta, \lambda_\gamma \in [0, 1)$, assuming the distance between any two points in the feasible convex region \mathcal{F} are bounded in infinity norm by D_∞ and in 2-norm by D , the regret is bounded by:

$$R(T) \leq \frac{G_\infty(D^2 + dD_\infty^2\sqrt{T})}{2\eta(1-\beta_1)} + \left(\frac{\beta_1\lambda_\beta d}{1-\lambda_\beta} + \frac{|\gamma|\lambda_\gamma d}{1-\lambda_\gamma} \right) \frac{G_\infty D_\infty}{1-\beta_1} + \frac{G_\infty \eta d \sqrt{T}}{(1-\beta_1)} (1 + |\gamma|)^2. \quad (10)$$

Proof. Recall the definition of regret,

$$R(T) = \sum_{t=1}^T [L_t(\theta_t) - L_t(\theta^*)]. \quad (11)$$

We can use Lemma C.1 to estimate each term in $R(T)$,

$$L_t(\theta_t) - L_t(\theta^*) \leq \langle g_t, \theta_t - \theta^* \rangle = \sum_{i=1}^d g_{t,i}(\theta_{t,i} - \theta_{i}^*). \quad (12)$$

The index i above refers to the i th element of a vector. We therefore have $R(T) \leq \sum_{t=1}^T \sum_{i=1}^d g_{t,i}(\theta_{t,i} - \theta_{i}^*)$.

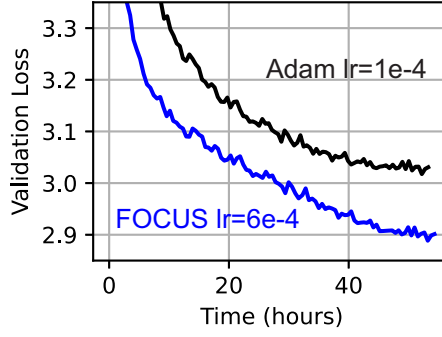


Figure 8. Adam and FOCUS have little difference in actual running time. We plot Figure 3c in terms of wall time rather than steps and find FOCUS needs a negligibly longer time to run the same 10^5 steps.

To study the term $g_{t,i}(\theta_{t,i} - \theta_{,i}^*)$, we make use of FOCUS updating rule,

$$\theta_{t+1} = \theta_t - \eta_t(\text{sign}(m_t) + \gamma_t \text{sign}(\theta_t - \hat{\theta}_t)), \quad (13)$$

which can also be written as

$$\theta_{t+1,i} = \theta_{t,i} - \eta_t \left(\frac{m_{t,i}}{|m_{t,i}|} + \gamma_t \frac{\theta_{t,i} - \hat{\theta}_{t,i}}{|\theta_{t,i} - \hat{\theta}_{t,i}|} \right). \quad (14)$$

Subtracting θ^* both sides and taking square, we have

$$\begin{aligned} (\theta_{t+1,i} - \theta_{,i}^*)^2 &= (\theta_{t,i} - \theta_{,i}^*)^2 - 2\eta_t(\theta_{t,i} - \theta_{,i}^*) \left(\frac{\beta_{1,t}m_{t-1,i} + (1 - \beta_{1,t})g_{t,i}}{|m_{t,i}|} + \gamma_t \frac{\theta_{t,i} - \hat{\theta}_{t,i}}{|\theta_{t,i} - \hat{\theta}_{t,i}|} \right) \\ &\quad + \eta_t^2 \left(\frac{m_{t,i}}{|m_{t,i}|} + \gamma_t \frac{\theta_{t,i} - \hat{\theta}_{t,i}}{|\theta_{t,i} - \hat{\theta}_{t,i}|} \right)^2. \end{aligned} \quad (15)$$

Rearranging the above equation, we can obtain

$$\begin{aligned} g_{t,i}(\theta_{t,i} - \theta_{,i}^*) &= \frac{|m_{t,i}|}{2\eta_t(1 - \beta_{1,t})} [(\theta_{t,i} - \theta_{,i}^*)^2 - (\theta_{t+1,i} - \theta_{,i}^*)^2] - \frac{\beta_{1,t}m_{t-1,i}}{1 - \beta_{1,t}}(\theta_{t,i} - \theta_{,i}^*) \\ &\quad - \frac{|m_{t,i}|\gamma_t}{1 - \beta_{1,t}}(\theta_{t,i} - \theta_{,i}^*) \frac{\theta_{t,i} - \hat{\theta}_{t,i}}{|\theta_{t,i} - \hat{\theta}_{t,i}|} + \frac{|m_{t,i}|\eta_t}{2(1 - \beta_{1,t})} \left(\frac{m_{t,i}}{|m_{t,i}|} + \gamma_t \frac{\theta_{t,i} - \hat{\theta}_{t,i}}{|\theta_{t,i} - \hat{\theta}_{t,i}|} \right)^2. \end{aligned} \quad (16)$$

Note that $\beta_{1,t} \leq \beta_1$, $\gamma_t \leq \gamma$, and the last term contains a sum of two sign functions, we have

$$\begin{aligned} g_{t,i}(\theta_{t,i} - \theta_{,i}^*) &\leq \frac{|m_{t,i}|}{2\eta_t(1 - \beta_1)} [(\theta_{t,i} - \theta_{,i}^*)^2 - (\theta_{t+1,i} - \theta_{,i}^*)^2] - \frac{\beta_{1,t}m_{t-1,i}}{1 - \beta_{1,t}}(\theta_{t,i} - \theta_{,i}^*) \\ &\quad - \frac{|m_{t,i}|\gamma_t}{1 - \beta_{1,t}}(\theta_{t,i} - \theta_{,i}^*) \frac{\theta_{t,i} - \hat{\theta}_{t,i}}{|\theta_{t,i} - \hat{\theta}_{t,i}|} + \frac{|m_{t,i}|\eta_t}{2(1 - \beta_{1,t})}(1 + |\gamma|)^2 \end{aligned} \quad (17)$$

To obtain the bound for $R(T)$, we need to study the summation over i and T for the four terms at the RHS of Equation (17).

The summation of the first term at the RHS of Equation (17) is

$$\begin{aligned}
 \sum_{i=1}^d \sum_{t=1}^T \frac{|m_{t,i}|}{2\eta_t(1-\beta_1)} [(\theta_{t,i} - \theta_{*,i}^*)^2 - (\theta_{t+1,i} - \theta_{*,i}^*)^2] &= \sum_{i=1}^d \frac{|m_{1,i}|}{2\eta(1-\beta_1)} (\theta_{1,i} - \theta_{*,i}^*)^2 \\
 &\quad + \sum_{i=1}^d \sum_{t=2}^T \frac{1}{2(1-\beta_1)} (\theta_{t,i} - \theta_{*,i}^*)^2 \left(\frac{|m_{t,i}|}{\eta_t} - \frac{|m_{t-1,i}|}{\eta_{t-1}} \right) \\
 &\leq \frac{G_\infty D^2}{2\eta(1-\beta_1)} + \sum_{i=1}^d \frac{1}{2\eta(1-\beta_1)} D_\infty^2 G_\infty \sqrt{T} \\
 &= \frac{G_\infty}{2\eta(1-\beta_1)} (D^2 + dD_\infty^2 \sqrt{T}), \tag{18}
 \end{aligned}$$

where we have used Lemma C.2 to bound $|m_{t,i}|$ and other assumptions on gradient norm as well as parameter range.

Similarly, the summation of the second term at the RHS of Equation (17) is

$$\sum_{i=1}^d \sum_{t=1}^T -\frac{\beta_{1,t}}{1-\beta_{1,t}} m_{t-1,i} (\theta_{t,i} - \theta_{*,i}^*) \leq \sum_{i=1}^d \sum_{t=1}^T \frac{\beta_1 \lambda_\beta^t}{1-\beta_1} G_\infty D_\infty \leq \frac{\beta_1 \lambda_\beta d}{(1-\beta_1)(1-\lambda_\beta)} G_\infty D_\infty. \tag{19}$$

And the third term leads to

$$\sum_{i=1}^d \sum_{t=1}^T -\frac{|m_{t,i}| \gamma_t}{1-\beta_{1,t}} (\theta_{t,i} - \theta_{*,i}^*) \frac{\theta_{t,i} - \hat{\theta}_{t,i}}{|\theta_{t,i} - \hat{\theta}_{t,i}|} \leq \frac{|\gamma| \lambda_\gamma d}{(1-\beta_1)(1-\lambda_\gamma)} G_\infty D_\infty. \tag{20}$$

The last term at the RHS of Equation (17) yields

$$\sum_{i=1}^d \sum_{t=1}^T \frac{|m_{t,i}| \eta_t}{2(1-\beta_{1,t})} (1+|\gamma|)^2 \leq \sum_{i=1}^d \frac{G_\infty \eta}{2(1-\beta_1)} (1+|\gamma|)^2 \sum_{t=1}^T \frac{1}{\sqrt{t}} \leq \frac{G_\infty \eta d \sqrt{T}}{(1-\beta_1)} (1+|\gamma|)^2. \tag{21}$$

Note that $R(T) \leq \sum_{t=1}^T \sum_{i=1}^d g_{t,i}(\theta_{t,i} - \theta_{*,i}^*)$, we combine the results from the four terms and can obtain Equation (10). \square